The International Journal of Cardiovascular Imaging (2019) 35:1473–1481
https://doi.org/10.1007/s10554-019-01602-z

ORIGINAL PAPER

Feasibility and utility of dual-energy chest CTA for preoperative planning in pediatric pulmonary artery reconstruction

Evan J. Zucker[1] · Aya Kino[1] · Heiko Schmiedeskamp[2] · Virginia Hinostroza[1] · Dominik Fleischmann[1] · Frandics P. Chan[1]

Received: 27 February 2019 / Accepted: 9 April 2019 / Published online: 23 April 2019

Abstract

The purpose of this study was to assess in pediatric pulmonary artery (PA) reconstruction candidates the feasibility and added utility of preoperative chest computed tomography angiography (CTA) using dual-energy technique, from which perfused blood volume (PBV)/iodine maps can be generated as a surrogate of pulmonary perfusion. Pediatric PA reconstruction patients were prospectively recruited for a new dose-neutral dual-energy CTA protocol. For each case, the severity of anatomic PA obstruction was graded by two pediatric cardiovascular radiologists in consensus using a modified Qanadli index. PBV maps were qualitatively reviewed and auto-segmented using Siemens *syngo*.via software. Associations between Qanadli scores and PBV were assessed with Spearman correlation (r) and ROC analysis. Effective radiation doses were estimated from dose-length product and ICRP 103 k-factors, using cubic Hermite spline interpolation. 19 patients were recruited with mean (SD) age of 6.0 (5.1), 11 (57.9%) female, 11 (73.7%) anesthetized. Higher QS correlated with lower PBV, both on a whole lung ($r = -0.54$, $p < 0.001$) and lobar ($r = -0.50$, $p < 0.001$) basis. The lung with lowest absolute PBV was predictive of the lung with highest Qanadli score, with AUC of 0.70 (95% CI 0.47–0.93). Qualitatively, PBV maps were heterogeneous, corresponding to multifocal PA stenoses, with decreased iodine content in areas of most severe obstruction. In conclusion, dual-energy chest CTA is feasible for pediatric PA reconstruction candidates. PBV maps show deficits in regions of more severe anatomic obstruction and may serve as a novel biomarker in this population.

Keywords Dual-energy · Pulmonary artery (PA) · Computed tomography angiography (CTA) · Perfused blood volume (PBV) · Iodine map · PA reconstruction

Introduction

Congenital pulmonary arterial (PA) abnormalities are a collectively rare form of congenital heart disease (CHD). However, they feature prominently in several disorders, namely ventricular septal defect (VSD) or tetralogy of Fallot (TOF) with pulmonary atresia and major aortopulmonary collaterals (MAPCAs) and primary PA stenosis associated with Williams and Alagille syndromes [1–7]. PA reconstruction refers to the technically challenging surgical process of attempting to normalize PA flow by augmenting all accessible PA branches to the segmental level. Where applicable, this may involve incorporation of MAPCAs into the PA circulation, a procedure known as unifocalization [1–6].

Due to the heterogeneous nature of PA anomalies and complexity of surgery, computed tomography angiography (CTA) has become a routine component of the preoperative evaluation. Indeed, modern CTA can now achieve diagnostic accuracy for assessing PA abnormalities similar to that of catheter angiography, the gold standard, at a fraction of the radiation dose [8–11]. Yet, while CTA provides excellent anatomic delineation, it generally cannot directly interrogate the physiologic significance of PA stenosis or atresia. Instead, other modalities such as nuclear lung perfusion scintigraphy or phase contrast (PC) magnetic resonance imaging (MRI) may be pursued for such noninvasive assessment [12].

In recent years, dual-energy CT (DECT) has gained traction as a novel method for supplementing traditional

✉ Evan J. Zucker
zucker@post.harvard.edu

[1] Department of Radiology, Stanford University School of Medicine, 725 Welch Road, Stanford, CA 94305, USA

[2] Siemens Medical Solutions USA, 40 Liberty Boulevard, Malvern, PA 19355, USA

anatomic CT. Using multiple tube voltages, DECT facilitates the generation of distinct beam energy spectra that permit more granular and quantitative material decomposition. In particular, the added diagnostic value of DECT is now well-established for pulmonary embolism (PE), in which DECT-derived pulmonary perfused blood volume (PBV) or iodine maps show regional deficits in lung iodine concentration in the distribution of PA emboli that align with perfusion defects on scintigraphy [13–16]. Furthermore, in animal models, PBV has been shown to correlate with more direct measurements of pulmonary blood flow (PBF) obtained through dynamic first-pass perfusion CT [17].

However, to our best knowledge, DECT has not been utilized previously for PA reconstruction candidates, in whom stenotic or atretic PA segments might similarly correspond to regionally decreased lung iodine concentration on PBV maps. The purpose of this study was to determine the feasibility and utility of dual-energy chest CTA for preoperative PA reconstruction planning and if the severity of anatomic obstruction correlates with PBV deficits, as a surrogate of pulmonary perfusion.

Materials and methods

This study was approved by the Institutional Review Board (IRB) and performed in accordance with Health Insurance Portability and Accountability Act (HIPAA) guidelines. Written informed consent was provided by patients ≥ age 18 or by a parent/guardian for pediatric subjects < age 18. In addition, written informed assent was obtained for child subjects ≥ age 7 and < age 18.

Study subjects

Patients undergoing preoperative planning CTA from February 1, 2017 through February 1, 2019 at a single tertiary care children's hospital in anticipation of elective PA reconstruction surgery were prospectively recruited. The additional subject inclusion criteria were: ability to obtain consent/assent and ability to perform a breath-held acquisition (either awake or under anesthesia). These criteria encompassed individuals with the following indications: isolated pulmonary artery stenosis, hypoplasia, or atresia; Williams or Alagille syndromes; TOF without or with absent pulmonary valve; and prior unifocalization with a PA conduit or central shunt. All demographic groups, including adults ages 18 or older being evaluated at the children's hospital, were eligible to participate in the study. The subject exclusion criteria were: known existence of > 1 source of pulmonary arterial supply, as in the case of uncorrected or residual MAPCAs; requirement for electrocardiographic (ECG)-gating, e.g., for concurrent detailed coronary evaluation; anticipation of emergency surgery; or inability to meet inclusion criteria. Demographic information, including age and gender, scan indications, and clinical/surgical history were recorded for each patient.

Image acquisition

All studies were performed on a dual-source 128-slice multidetector CT (MDCT) scanner (SOMATOM Definition Flash, Siemens Healthineers, Erlangen, Germany) using a newly developed dual-energy chest CTA protocol, in lieu of the departmental standard, a spiral, non-gated, high-pitch (Flash mode) acquisition. Scan parameters were adjusted to maintain dose neutrality with the conventional technique according to patient weight and consisted of the following: tube A-80 kilovoltage peak (kVp)/150–200 reference milliampere-seconds (mAs); tube B-Sn140 kVp/64–85 reference mAs; pitch: 0.7. The slice collimation and gantry rotation time were 64 × 0.6 mm and 0.28 s, respectively.

Patients were imaged supine with both arms extended above the head. Scans were performed in the craniocaudal direction at end-inspiration. Anatomic coverage extended from the level of the thoracic inlet to the level of the diaphragm, planned from initial lateral and frontal scout topograms. Using bolus tracking, acquisitions were manually triggered at the qualitative peak enhancement of the main PA (or right ventricle, if the main PA was absent or otherwise non-evaluable) as determined by the supervising pediatric cardiovascular radiologist present during the acquisition.

All acquisitions were performed after intravenous (IV) administration of a nonionic contrast medium at a dose of 2 mL/kg (not to exceed 120 mL), followed by a 1 mL/kg saline flush (not to exceed 20 mL), delivered via a power injector (MEDRAD Stellant D Injection System, Bayer HealthCare, Whippany, NJ). The default contrast agent was the low osmolar Omnipaque (Iohexol) 350 (GE Healthcare, Chicago, IL). Due to its purportedly less nephrotoxic and local warmth-inducing properties, iso-osmolar Visipaque (Iodixanol) 320 (GE Healthcare, Chicago, IL) was substituted in patients who had a history of renal impairment or were non-anesthetized and appeared anxious on assessment by a child life specialist [18, 19]. A 20–24 gauge (G) IV, the caliber dependent on patient weight, was placed either in a foot vein when feasible for anesthestized patients less than 9-years-old to minimize streak artifact from a dense contrast bolus in the superior vena cava (SVC) or else in an antecubital vein, preferably on the right. The injection flow rate was adjusted by the supervising pediatric cardiovascular radiologist to maintain a 15–20 s contrast bolus duration while not exceeding the maximum injection pressure. When required, sedative medications were administered at the discretion of the supervising pediatric cardiovascular anesthesiologist, utilizing IV propofol (bolus totaling 10–80 mg and/

or infusion at 150–250 mcg/kg/min), IV succinylcholine (up to 20 mg), IV ketamine (10–20 mg), inhaled sevoflurane (0.2–7.1%), inhaled nitrous oxide (0.15–4.7 L/min), and/or intranasal dexmedetomidine (up to 45 mcg), as deemed indicated.

Image post-processing

CT datasets were reconstructed at the scanner console to axial 0.75–1.5 mm slice thickness using an iterative algorithm (ADMIRE, Siemens Healthineers, Erlangen, Germany) and a medium-soft convolutional kernel with edge-preserving noise reduction (I26). Mixing ratios of 60% 80 kVp/40% Sn140 kVp were utilized in addition to pure tube A (80 kVp) and pure tube B (Sn140 kVp) reconstructions. Multiplanar reformats (MPRs) and maximum intensity projection (MIPs) were also generated. The images were then transmitted to the picture archiving and communication system (Centricity PACS, GE Healthcare, Chicago, IL) and Aquarius iNtuition software (TeraRecon, Foster City, CA) for anatomic visualization in addition to *syngo*.via software (Siemens Healthineers, Erlangen, Germany) for further review and dual-energy analysis.

In *syngo*.via, using the "DE Dense Lung" application with default settings, PBV/iodine maps were generated for each acquisition, normalized to the Hounsfield unit (HU) attenuation of a circular region of interest (ROI) manually drawn in the main PA. The lungs were segmented automatically using built-in features. Quantitative evaluation tools were then utilized to generate the mean standard deviation (SD) absolute HU attenuation of the combined lungs as well as each individual lung and lobe. The percent enhancement of each of these anatomical regions relative to the main PA ROI was also provided (Fig. 1).

Image assessment

For each case, two pediatric cardiovascular radiologists (E.J.Z. and A.K., with 6 and 12 years of post-residency experience, respectively), blinded to patient information and PBV maps, in consensus graded the severity of anatomic PA obstruction. This grading was performed using a modified Qanadli index, adapted from studies of pulmonary embolism [20]. Each segmental PA branch (20 per patient) was scored on the following ordinal scale: 0: no stenosis; 1: < 50% stenosis; 2: 50–69% stenosis; 3: ≥ 70% stenosis. Drawing on the Qanadli methodology, if a proximal obstruction was present (i.e., at the level of the main right or left PA or an interlobar or lobar PA branch), all segmental PA branches were assigned a score at least as severe as would be assigned for the more proximal branch, even if distal branches were not as diseased. If the severity of disease was greater in the segmental branch compared to more proximal branches, the segment was assigned the higher score, based on its degree of stenosis. Absent, atretic, or occluded segments were assigned the highest score of 3. The left upper and bilateral lower lobes could each be assigned 0–15 points, while the right upper and middle lobes could be assigned 0–9 and 0–6 points, respectively, accounting for the number of segments in each lobe. Each lung could be assigned 0–30 points, for a total possible score of 0–60.

Anatomic images were first reviewed in PACS, with reference to MPRs and MIPs if needed. If further clarification was required, additional reformats were generated in Aquarius iNtuition. PBV maps were then qualitatively reviewed in *syngo*.via to assess visual correlations between the severity and pattern of anatomic obstruction and regional deficits in lung iodine content.

Radiation dose assessment

For each dual-energy acquisition, the scan dose-length (DLP) product was recorded from the scanner console. Effective radiation dose (ED) in millisieverts (mSv) was then estimated as the product of DLP and a conversion factor (k) for the chest based on patient age. The k-factors were obtained from the International Commission on Radiological Protection (ICRP) publication 103 [21]. Because this document only supplies k-factors for several discrete ages, conversion factors for unspecified ages were interpolated with the cubic Hermitte spline method using MATLAB software (version R2014a, MathWorks, Natick, MA) [22]. The "adult" k-factor was used for all patients ≥ age 18. To provide the most conservative (maximal) estimate of ED, k-factors at 80 kVp, which are numerically the highest, were utilized. Any unanticipated repeat acquisitions were also tracked.

Statistical analysis

Three PBV indices were constructed: (1) mean absolute enhancement in HU of the combined lungs and of each lung and lobe; (2) percent enhancement of the combined lungs and of each lung and lobe relative to that of the main PA; and (3) mean absolute enhancement in HU of each lung and lobe ÷ mean absolute enhancement of the combined lungs in HU. The latter metric was included recognizing that non-normalized absolute lung/lobe enhancement and the degree of main PA enhancement could be variable in this diverse patient cohort. Thus, expressing lung and lobar mean HU enhancement as a fraction of the combined lung mean HU enhancement was anticipated to better discern regional differences in iodine content. Spearman correlation (r) was used to assess associations between Qanadli scores (QSs) and each PBV index. In addition, nonparametric receiver operating characteristic (ROC) curve analysis was performed to determine

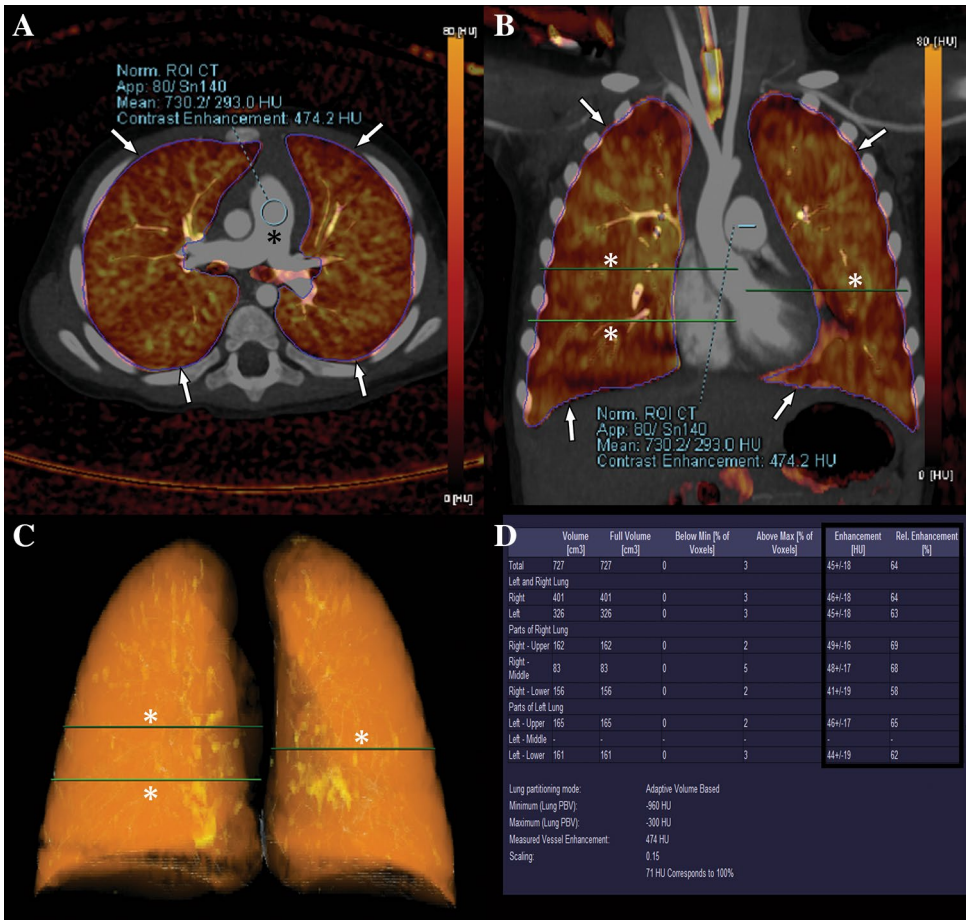

Fig. 1 Example PBV image analysis in a 1-year-old female post congenital pulmonary airway malformation (CPAM) resection with normal PAs and a modified Qanadli score of 0. Selected **a** axial and **b** coronal fused anatomic/PBV images as well a **c** three-dimensional PBV map and **d** corresponding quantitative output in the *syngo*.via environment are shown. The PBV maps are normalized to a circular region of interest manually drawn in the main PA (black asterisk), **a** and displayed on a 0–80 HU scale. After automated lung segmentation is performed, bounding contours are generated, delineating the borders of the lungs (arrows, **a** and **b**) and separation between lobes (white asterisks, **b** and **c**). The automated quantitative evaluation tool output (boxed columns, **d**) includes the mean SD absolute HU of the combined lungs as well as of each lung and lobe (defined by the bounding contours and by default scaled to 15% of their actual values) in addition to the % enhancement relative to that of the normalization ROI (black asterisk, **a**)

if, for each patient, the lung with the lowest PBV indices was predictive of the lung with highest QS. Cases in which both lungs had the same QS were excluded from the analysis.

Statistical analysis was performed using Microsoft Excel (version 2016, Microsoft Corporation, Redmond, WA) and Stata software (version 14, StataCorp LP, College Station, TX). Statistical significance was set at the $p \leq 0.05$ level. Percentages were rounded to the nearest 10th of a percent.

Results

The final study cohort consisted of 19 patients; subject demographics and scan indications are summarized in Table 1. Mean SD scan time, ED, and total QS were 2.2 ± 0.8 s, 1.7 ± 0.5 mSv, and 34.6 ± 12.4, respectively. All studies were diagnostic for clinical purposes; no repeat acquisitions were required. In one case, pure 80/Sn140 kVp reformats, which are required to generate PBV maps, were not created at the time of acquisition and could not subsequently be obtained at the scanner console due to an idiosyncratic data storage fault. Therefore, this exam was excluded from PBV analysis.

Results of the correlation analysis between PBV indices and Qanadli scores are summarized in Table 2. Higher QS correlated with lower PBV enhancement in HU, normalized to the average HU enhancement of the combined lungs (index #3), both on a whole lung ($r = -0.54$, $p < 0.001$) and lobar ($r = -0.50$, $p < 0.001$) basis. There was no statistically significant correlation between QS and absolute enhancement in HU or percent enhancement relative to the main PA

Table 1 Summary characteristics of the study patient cohort

Total recruitment	$N = 19$
Age	
Mean ± SD	6.0 ± 5.1 years
Range	1.1–18.8 years
Gender	
Female	11 (57.9%)
Male	8 (42.1%)
Anesthesia	
Yes	14 (73.7%)
No	5 (26.3%)
Indications	
Redo unifocalization	10 (52.6%)
TOF with PA stenosis	3 (15.8%)
Primary PA stenosis	5 (26.3%)
Post-op CPAM	1 (5.3%)

N number, *SD* standard deviation, *TOF* tetralogy of Fallot, *PA* pulmonary artery, *CPAM* congenital pulmonary airway malformation

(indices #1 and #2, respectively), whether on a combined lung, individual lung, or lobar basis.

Results of the ROC curve analysis are shown in Fig. 2; supporting raw data are shown in Table 3. The lung with lowest PBV indices was predictive of the lung with highest QS with a sensitivity of 77.8%, specificity of 62.5%, and AUC of 0.70 (95% CI 0.47–0.93). All PBV indices, for a given patient, are multiplicative transformations of each other; therefore, their ROC curves were identical for predicting the lung with greatest anatomic obstruction based on the lung with lowest PBV values.

Qualitatively, PBV maps were heterogeneous, corresponding to multifocal PA stenoses. There was visually decreased iodine content in areas of most severe obstruction. Such iodine deficits were most pronounced in the case of unilateral PA absence or asymmetric severe stenosis (Fig. 3) but also observed on a regional (e.g., lobar) basis (Fig. 4).

Discussion

In this study, we have demonstrated the feasibility of dual-energy CTA for preoperative planning in pulmonary artery reconstruction. There was a moderate negative correlation between the severity of anatomic obstruction, as assessed by a modified Qanadli index, and the degree of PBV enhancement in HU normalized to the overall enhancement of the lungs in each patient. This relationship persisted both on a whole lung and lobar basis. In addition, the lung with lower PBV enhancement was predictive of the lung with more severe Qanadli obstruction. Finally, there was visual confirmation of iodine deficits in areas of significant anatomic obstruction.

Our findings support the hypothesis that relative deficits in PBV maps in PA stenosis or atresia are reflective of regionally impaired pulmonary perfusion related to anatomic obstruction, similar to what has been observed in pulmonary embolism. The presence of only moderate correlation is likely multifactorial, related to the relative imprecision of the modified Qanadli scoring system, heterogeneous and multifocal nature of disease, and potential for alternative pathways of pulmonary blood flow, augmenting or bypassing the PA circulation. Moreover, it is also possible that some apparently severe anatomic stenoses are not associated with as compromised perfusion as might be anticipated. Finally, while iodine content is a recognized surrogate for pulmonary blood flow based on prior DECT studies, it is not identical to it [14, 17].

Considering the heterogeneous physiology of patients in this study and individualization of contrast injection profiles, the lack of a significant correlation between anatomic

Table 2 Correlation between Qanadli scores and pulmonary blood volume (PBV) indices

PBV index	Anatomical group	r	p-value
Mean absolute enhancement (HU)	Combined lungs	0.36	0.15
Mean absolute enhancement (HU)	Individual lung	−0.01	0.97
Mean absolute enhancement (HU)	Individual lung lobe	−0.05	0.67
% Enhancement relative to main PA enhancement	Combined lungs	0.18	0.48
% Enhancement relative to main PA enhancement	Individual lung	−0.08	0.63
% Enhancement relative to main PA enhancement	Individual lung lobe	−0.14	0.20
Mean absolute enhancement (HU) ÷ mean absolute enhancement (HU) of combined lungs	Individual lung	−0.54	$p < 0.001^{\dagger}$
Mean absolute enhancement (HU) ÷ mean absolute enhancement (HU) of combined lungs	Individual lung lobe	−0.50	$p < 0.001^{\dagger}$

r coefficients correspond to the degree of correlation between the PBV index and the absolute total Qanadli score of the anatomical group under consideration

r Spearman correlation coefficient, *HU* Hounsfield unit

$^{\dagger}p \leq 0.05$

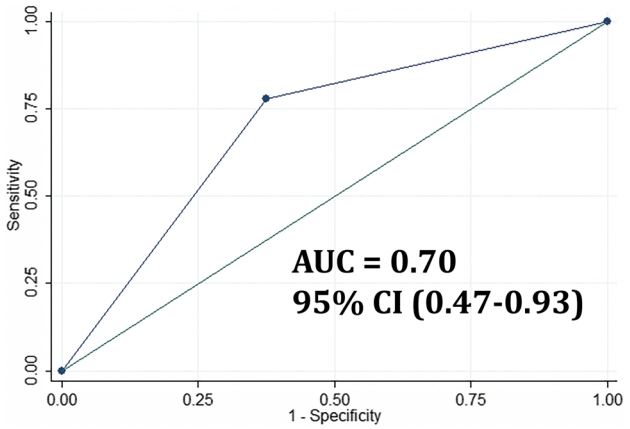

Fig. 2 ROC curve illustrating the diagnostic performance of using PBV enhancement to determine the lung with greatest anatomic obstruction. The lung with lowest absolute PBV enhancement (relative to the contralateral lung in each patient) was predictive of the lung with highest modified Qanadli score with an AUC of 0.70 (95% CI 0.47–0.93)

Table 3 PBV versus modified Qanadli score prediction of most obstructed lung

	Right lung highest QS	Left lung highest QS
Right lung lowest PBV enhancement	*N* = 4 (A)	*N* = 2 (B)
Left lung lowest PBV enhancement	*N* = 3 (C)	*N* = 8 (D)

Accuracy = (A + D) / (A + B + C + D) = 70.6% correctly classified. Of 19 patients, one was excluded from this analysis due to QS = 0 and a second due to unprocessable PBV maps related to a data storage fault. The latter case involved a unilateral absent left pulmonary artery, and its inclusion most likely would have further increased the accuracy of PBV for predicting anatomic obstruction due to the marked asymmetry of disease

PBV perfused blood volume, *QS* modified Qanadli score

severity scores and uncorrected absolute lung enhancement or enhancement relative to the main PA is not surprising. For example, the peak enhancement of the main PA achieved differs among patients; thus, lung enhancement relative to the main PA could increase simply because a lower peak main PA enhancement was achieved. Thus, normalizing to the absolute enhancement of the combined lungs helped establish a more relevant "baseline" in each patient when assessing correlations with a constant anatomic scale. However, on a patient-specific basis, relative differences in absolute enhancement could be used to help predict the lung with more severe anatomic disease.

Ultimately, the availability of PBV maps in pulmonary artery reconstruction patients poses several potential opportunities. First, PBV maps, if available at baseline and in follow-up after surgery, could provide new metrics of disease severity and subsequent improvement, potentially enhancing risk prediction. Second, PBV maps might facilitate prediction of the most hemodynamically significant PA abnormalities and thus the optimal targets for intervention. Indeed, some seemingly high-grade PA stenoses may not be clinically relevant, while at the same time, significant perfusion deficits could occur in the face of mild or even subclinical anatomic disease. Finally, if PBV maps sufficiently correlated with lung perfusion metrics obtained by other modalities, dual-energy CTA could potentially provide a "one-stop shop" for assessment of anatomy and pulmonary blood flow, obviating the need for other imaging tests in many patients. Thus, initial future directions would focus on validating PBV data using other imaging exams (e.g., nuclear scintigraphy, PC-MRI with magnetic resonance angiography [MRA], catheter angiography) and assessing its prognostic value.

The decision to clinically implement a dual-energy CTA protocol for PA reconstruction planning must weigh the benefits of the additional data against several factors. Ionizing radiation dose is always of utmost concern, particularly in children who are most radiosensitive. Nevertheless, a dose-neutral protocol, with low doses estimated on average < 2 mSv, was successfully achieved in this cohort while preserving sufficient diagnostic anatomic information. Another consideration is speed. Scan speeds with the DE CTA protocol averaged 2.2 s. To best ensure diagnostic anatomic imaging, all DE CTAs were performed breath-held. In contrast, in our experience, high-pitch acquisitions on the same scanner in similar patients are generally sub-second exams and often adequate for assessment of PA anatomy when performed free-breathing. Patients who could not breath-hold but otherwise did not require anesthesia to limit patient motion were not enrolled in this study and instead scanned with the traditional protocol. It is not known whether image quality would have been sufficient without this breath-holding requirement. Nevertheless, it is notable that the scan times achieved in our study using a second-generation dual-source CT in dual-energy mode are comparable to those attainable with the more widely available conventional single-energy spiral CT [23, 24]. Moreover, third-generation dual-source and emerging scanners are capable of > 3 times faster imaging speeds compared to second-generation dual-source scanners [25, 26]. Thus, for subjects with similar body sizes, it is anticipated that sub-second chest CTA exams could also be achieved in dual-energy mode with newer scanners, facilitating free-breathing technique while obviating respiratory motion concerns.

Our study has several limitations. First, this pilot study included a heterogeneous patient population, many with multifocal obstructive anatomic PA disease, from a single

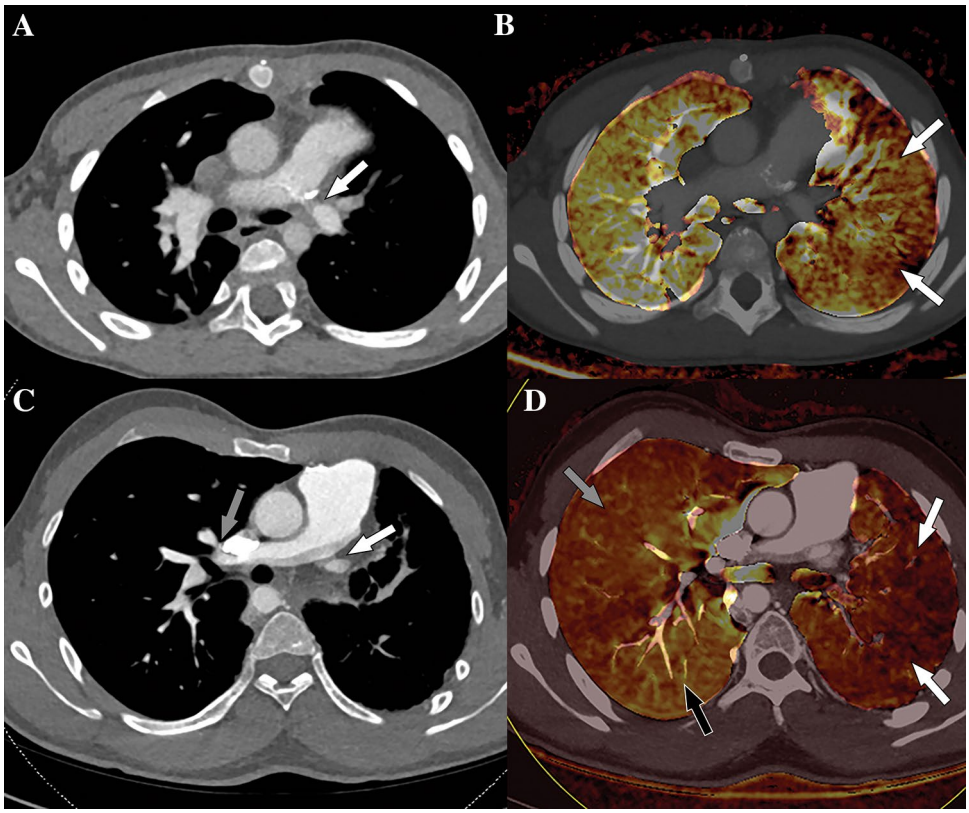

Fig. 3 Examples of whole-lung PBV deficits in **a**, **b** a 2-year-old male and **c**, **d** an 18-year-old male, both with TOF, undergoing DE chest CTA prior to pulmonary artery reconstruction. **a** Axial contrast-enhanced CT image shows a severe stenosis (arrow) at the origin of the left PA. **b** Corresponding fused anatomic/PBV image shows asymmetric decreased perfusion (arrows) of the entire left lung. **c** Axial contrast-enhanced enhanced CT image shows absence of the left PA (white arrow) with tiny mediastinal collaterals and a small left hemithorax. Multiple right-sided PA stenoses were also present with upper lobe predominance (gray arrow-example). **d** Corresponding fused anatomic/PBV image shows heterogeneous lung perfusion that is overall decreased on the left (white arrows) compared to the right. In addition, there is lesser perfusion of the right upper lobe (gray arrow), compared to the right lower lobe (black arrow), concordant with the pattern of anatomic PA obstruction

institution without long-term follow-up. Nonetheless, we demonstrated a quantitative and qualitative correlation between PBV deficits and stenosis severity in a broad range of prospectively enrolled subjects, thus serving as a proof concept for the potential utility of PBV maps in this context. Second, the modified Qanadli scoring method provides only a broad overview of often diverse anatomic obstruction but is nonetheless supported by a similar use in pulmonary embolism studies [14–16]. However, additional validation is still needed in the context of pulmonary artery reconstruction to determine threshold scores that might suggest more clinically significant disease and could then be further correlated with PBV parameters. Third, consensus rather than individual scoring was chosen due to the complexity and heterogeneity of PA disease. As such, it is not possible to perform interobserver agreement analysis of the modified scoring system. Fourth, a variety of other PBV metrics are possible but those used were developed to allow measureable correlation between anatomical obstruction and iodine deficits. For example, more intricate predictive modeling from PBV parameters might incorporate the volume of a lung, lobe, or segment supplied by a particular PA distribution. Fifth, as previously detailed, a breath-holding requirement was imposed that decreased potential recruitment; assessment of non-breath-held exams and dual-energy acquisitions on later-generation scanners may be fruitful for future study. Finally, contemporaneous imaging modalities (e.g., scintigraphy, PC-MRI with MRA, Doppler ultrasound) performed near to the time of the CTs were not sufficiently available. Therefore, correlative evaluation could not be specifically performed, although this is also an area for potential investigation.

In conclusion, we have demonstrated the feasibility of dual-energy chest CTA as a successful alternative for preoperative planning in PA reconstruction. PBV deficits correlate with more severe anatomic obstruction. Ultimately, PBV maps facilitated by dual-energy CTA may help improve identification of the most heavily diseased

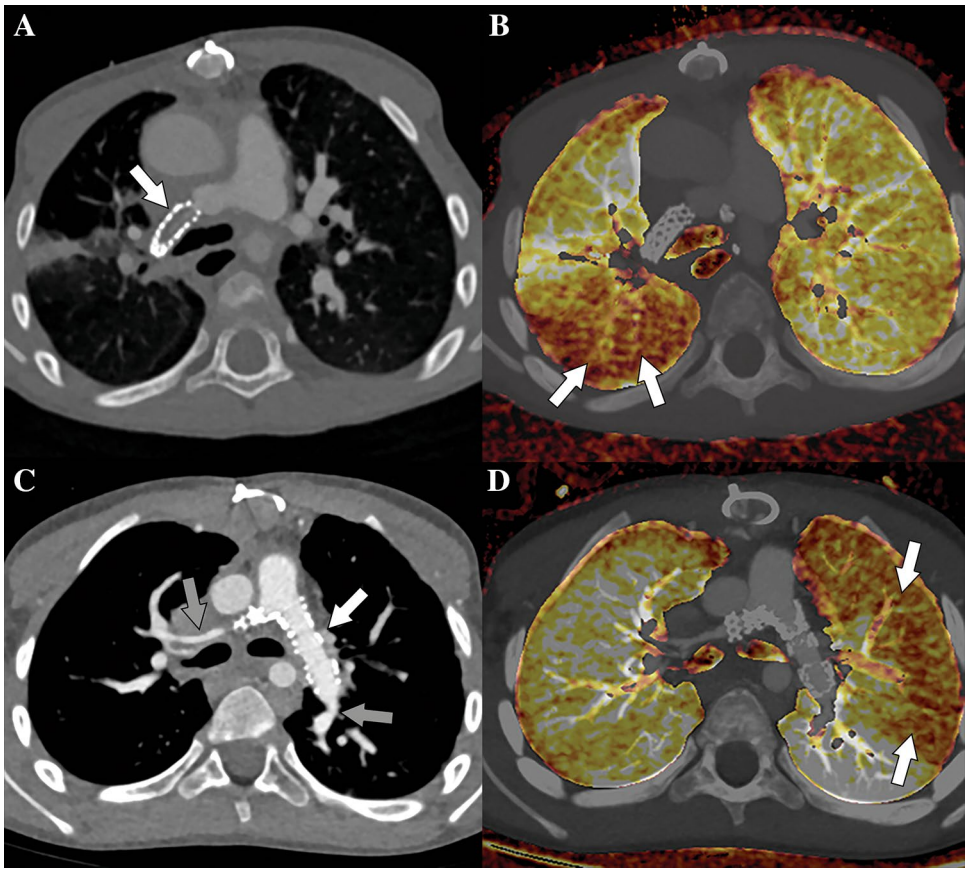

Fig. 4 Examples of regional PBV deficits in **a**, **b** a 6-year-old male and **c**, **d** a 5-year-old male, both with TOF/pulmonary atresia and prior unifocalization, undergoing DE chest CTA prior to pulmonary artery reconstruction. **a** Axial contrast-enhanced CT image shows subtotal occlusion (arrow) of a PA stent supplying the posterior right upper lobe. **b** Corresponding fused anatomic/PBV image shows regionally decreased perfusion (arrows) in the matching lung territory. **c** Axial contrast-enhanced enhanced CT image shows absence of the left upper PA branches at their expected convergence with the main left PA (white arrow), which are jailed by a left PA stent and occluded. Additional multifocal PA hypoplasia and stenoses are present (gray arrows-examples). **d** Corresponding fused anatomic/PBV image shows least perfusion of the left upper lobe (white arrows), corresponding to the area of most severe anatomic PA obstruction

PA segments and serve as novel qualitative and quantitative prognostic biomarker in this complex and often tenuous patient population.

Author Contributions Guarantors of integrity of entire study: E.J.Z.; study concepts/study design: E.J.Z., D.F., F.P.C.; data acquisition or data analysis/interpretation: all authors; manuscript drafting: E.J.Z.; manuscript revision for important intellectual content: all authors; approval of final version of submitted manuscript: all authors.

Compliance with ethical standards

Conflict of interest E.J.Z., A.K., V.H., D.F., F.P.C.: no relevant relationships. H.S.: employed by Siemens Medical Solutions USA.

Ethical approval All procedures performed in studies involving human participants were in accordance with the ethical standards of the institutional and/or national research committee and with the 1964 Helsinki declaration and its later amendments or comparable ethical standards.

Informed consent Informed consent was obtained from all individual participants included in the study (or their parent/guardian for pediatric subjects less than age 18-years-old).

References

1. Mainwaring RD, Ibrahimiye AN, Hanley FL (2016) Surgical technique for repair of peripheral pulmonary artery stenosis and other complex peripheral reconstructions. Ann Thorac Surg 102(2):e181–e183
2. Carrillo SA, Mainwaring RD, Patrick WL et al (2015) Surgical repair of pulmonary atresia with ventricular septal defect and major aortopulmonary collaterals with absent intrapericardial pulmonary arteries. Ann Thorac Surg 100(2):606–614
3. McElhinney DB, Reddy VM, Hanley FL (1998) Tetralogy of Fallot with major aortopulmonary collaterals: early total repair. Pediatr Cardiol 19(4):289–296
4. Ikai A (2018) Surgical strategies for pulmonary atresia with ventricular septal defect associated with major aortopulmonary collateral arteries. Gen Thorac Cardiovasc Surg 66(7):390–397
5. Mainwaring RD, Patrick WL, Ma M, Hanley FL (2018) An analysis of patients requiring unifocalization revision following midline unifocalization for pulmonary atresia with ventricular septal defect and major aortopulmonary collaterals. Eur J Cardiothorac Surg 54(1):63–70
6. Asija R, Hanley FL, Roth SJ (2013) Postoperative respiratory failure in children with tetralogy of Fallot, pulmonary atresia, and major aortopulmonary collaterals: a pilot study. Pediatr Crit Care Med 14(4):384–389

7. Smith NE, Fabian T, Nabagiez J (2018) Unilateral pulmonary artery atresia in an adult: a case report. Respir Med Case Rep 26:105–107
8. Meinel FG, Huda W, Schoepf UJ et al (2013) Diagnostic accuracy of CT angiography in infants with tetralogy of Fallot with pulmonary atresia and major aortopulmonary collateral arteries. J Cardiovasc Comput Tomogr 7(6):367–375
9. Lloyd DFA, Goreczny S, Austin C et al (2018) Catheter, MRI and CT imaging in newborns with pulmonary atresia with ventricular septal defect and aortopulmonary collaterals: quantifying the risks of radiation dose and anaesthetic time. Pediatr Cardiol 39(7):1308–1314
10. Lin MT, Wang JK, Chen YS et al (2012) Detection of pulmonary arterial morphology in tetralogy of Fallot with pulmonary atresia by computed tomography: 12 years of experience. Eur J Pediatr 171(3):579–586
11. Jia Q, Cen J, Li J et al (2018) Anatomy of the retro-oesophageal major aortopulmonary collateral arteries in patients with pulmonary atresia with ventricular septal defect: results from preoperative CTA. Eur Radiol 28(7):3066–3074
12. Yatsuyanagi E, Sato K, Kikuchi K, Saito H (2014) Pulmonary blood flow measurement using magnetic resonance imaging (MRI) without contrast medium;comparison of phase contrast MRI and perfusion-ventilation scintigraphy. Kyobu Geka 67(2):100–104
13. Kay FU, Beraldo MA, Nakamura MAM et al (2018) Quantitative dual-Energy computed tomography predicts regional perfusion heterogeneity in a model of acute lung injury. J Comput Assist Tomogr 42(6):866–872
14. Thieme SF, Becker CR, Hacker M, Nikolaou K, Reiser MF, Johnson TR (2008) Dual energy CT for the assessment of lung perfusion–correlation to scintigraphy. Eur J Radiol 68(3):369–374
15. Thieme SF, Johnson TR, Lee C et al (2009) Dual-energy CT for the assessment of contrast material distribution in the pulmonary parenchyma. AJR Am J Roentgenol 193(1):144–149
16. Cai XR, Feng YZ, Qiu L et al (2015) Iodine distribution map in dual-energy computed tomography pulmonary artery imaging with rapid kVp switching for the diagnostic analysis and quantitative evaluation of acute pulmonary embolism. Acad Radiol 22(6):743–751
17. Fuld MK, Halaweish AF, Haynes SE, Divekar AA, Guo J, Hoffman EA (2013) Pulmonary perfused blood volume with dual-energy CT as surrogate for pulmonary perfusion assessed with dynamic multidetector CT. Radiology 267(3):747–756
18. Zhang J, Jiang Y, Rui Q et al (2018) Iodixanol versus iopromide in patients with renal insufficiency undergoing coronary angiography with or without PCI. Medicine (Baltimore) 97(18):e0617
19. Lubbers MM, Kock M, Niezen A et al (2018) Iodixanol versus iopromide at coronary CT angiography: lumen opacification and effect on heart rhythm-the randomized IsoCOR trial. Radiology 286(1):71–80
20. Qanadli SD, El Hajjam M, Vieillard-Baron A et al (2001) New CT index to quantify arterial obstruction in pulmonary embolism: comparison with angiographic index and echocardiography. AJR Am J Roentgenol 176(6):1415–1420
21. Deak PD, Smal Y, Kalender WA (2010) Multisection CT protocols: sex- and age-specific conversion factors used to determine effective dose from dose-length product. Radiology 257(1):158–166
22. Ghoshhajra BB, Lee AM, Engel LC et al (2014) Radiation dose reduction in pediatric cardiac computed tomography: experience from a tertiary medical center. Pediatr Cardiol 35(1):171–179
23. Siemens Healthineers (2019) SOMATOM definition flash. https://static.healthcare.siemens.com/siemens_hwem-hwem_ssxa_websites-context-root/wcm/idc/groups/public/@global/@imaging/@ct/documents/download/mdaw/mzcz/~edisp/ct_ws_somatom_definition_flash_international-00292513.pdf. Accessed February 22, 2019.
24. De Zordo T, von Lutterotti K, Dejaco C et al (2012) Comparison of image quality and radiation dose of different pulmonary CTA protocols on a 128-slice CT: high-pitch dual source CT, dual energy CT and conventional spiral CT. Eur Radiol 22(2):279–286
25. Siemens Healthineers (2019) SOMATOM force. https://static.healthcare.siemens.com/siemens_hwem-hwem_ssxa_websites-context-root/wcm/idc/groups/public/@global/@imaging/@ct/documents/download/mda4/ndqx/~edisp/di_ct_brochure_somatom_force_brochure_07-2018-05556644.pdf. Accessed February 22, 2019
26. Abdellatif W, Nicolaou S, Schmiedeskamp H, Powell J (2018) Multifactorial comparative study of dual source CT scanners in acute pulmonary embolism. Paper presented at the 104th annual meeting of the radiological society of North America (RSNA), Chicago, IL, November 26, 2018